Interaction of High-Speed Compressible Viscous Flow and Structure by Adaptive Finite Element Method

Wiroj Limtrakarn
Mechanical Engineering Department, Thammasat University, Bangkok 12120, Thailand
Pramote Dechaumphai*
Mechanical Engineering Department, Chulalongkorn University, Bangkok 10330, Thailand

Interaction behaviors of high-speed compressible viscous flow and thermal-structural response of structure are presented. The compressible viscous laminar flow behavior based on the Navier-Stokes equations is predicted by using an adaptive cell-centered finite-element method. The energy equation and the quasi-static structural equations for aerodynamically heated structures are solved by applying the Galerkin finite-element method. The finite-element formulation and computational procedure are described. The performance of the combined method is evaluated by solving Mach 4 flow past a flat plate and comparing with the solution from the finite different method. To demonstrate their interaction, the high-speed flow, structural heat transfer, and deformation phenomena are studied by applying the present method to Mach 10 flow past a flat plate.

Key Words: Flow-Structure Interaction, Aerodynamic Heating Rate, Adaptive Mesh

Nomenclature

Ae : element area
$[A^*]$: Jacobian matrix
$\{E_F\}$: fluid flux vector in x direction
$\{E_T\}$: thermal flux vector in x direction
$\{F_F\}$: fluid flux vector in y direction
$\{F_T\}$: thermal flux vector in y direction
c : specific heat of structure
c_V : specific heat at constant volume of fluid
$\{\bar{G}_I\}$: average inviscid flux vector
$\{\bar{G}_V\}$: average viscous flux vector
$\{h_1, h_2\}$: element sizes
$\hat{n}$: unit normal vector
p : pressure
x, y : coordinate directions
X, Y : principle directions
$\{u, v\}$: x and y velocity components
$\{U_F\}$: fluid conservation variable vector
$\{U_T\}$: thermal conservation variable vector
$\{U_S\}$: nodal displacement vector
Γ_e : element boundary
Ω : element domain
δ : length of element sides
ε : total energy
λ_1, λ_2 : absolute second derivatives
ρ : density

* Corresponding Author,
E-mail : fmepdc@eng.chula.ac.th
TEL : +82-63-290-1473; **FAX** : +82-63-291-9312
Mechanical Engineering Department, Chulalongkorn University, Bangkok 10330, Thailand (Manuscript **Received** March 2, 2002; **Revised** September 27, 2004)

1. Introduction

Fluid-Thermal-Structural analysis methods have an important role in the design of high-speed flight vehicles, such as hypersonic air-breathing vehicles (Glass et al., 2002), for predicting vehicles' aerothermostructural performance. Significant coupling occurs between high-speed flow phenomena, aerodynamic heating rates on structural surfaces, structural temperature and their gradients, as well as structural deformations and stresses, creating multidisciplinary interaction phenomena. High-speed flow phenomena normally include complex flow characteristics, such as shock waves, shock-shock inter-

actions, thin boundary layers and shock-boundary layer interactions (Anderson, 1982; Anderson, 1991). Such phenomena have been studied by a number of researchers using both the numerical simulations and experimental techniques. These include, as few examples, the study of shock motion by self-induced oscillation of an expanded jet impinging on a cylinder (Kim et al, 2002), the experimental study for the flow characteristic of the supersonic dual coaxial free jet (Baek et al, 2003), and the numerical simulation of shock wave propagation using the lattice Boltzmann method (Kang et al, 2003). Some of these characteristics, especially near the structural surface, generate aerothermal load to vehicle structure, and normally affect the structural temperature, deformation and stress. Under intense aerodynamic heating rate, structural temperature begins to rise within few seconds and significant deformation may occur. In addition, the deformed structure may significantly alter the high-speed flow behavior and thus the aerothermal loads. These coupled effects indicate that the analysis of high-speed flow-structure interaction is an important consideration to high-speed vehicle design. Such coupled effects have been studied by a number of researchers recently. Computational fluid and structural dynamics commercial programs were combined together for predicting the flow and structure behaviors (Baum, 2002; Lohner et al., 2003). A parallel multilevel method for adaptively refined grids was introduced (Aftosmis et al., 2000) to reduce the overall computational effort. Embedded boundaries between the flow and the structure were proposed to effectively transfer information between the two different disciplines. The approach was later extended for unstructured grids to minimize the computational time and memory required for the flow analysis. The examples presented in these references, however, do not include the thermal response of the structure due to the intense aerodynamic heating rate from the high-speed flow.

In the present paper, an integrated flow-thermal-structural analysis approach for predicting each disciplinary behavior and their interaction is presented. The study of the interactions is a preliminary, but important, step toward the objectives of analyzing more realistic structures, such as thermal protection systems and scramjet engine structures. For high-speed compressible flows, the cell-centered finite-element method (Gnoffo, 1986; Dechaumphai and Limtrakarn, 1999) is combined with an adaptive meshing technique to solve the Navier-Stokes equations. Based on the solution obtained from the previous mesh that could be either the initial or adaptive mesh constructed earlier, the adaptive meshing technique generates an entirely new mesh that consists of small elements in the regions with large change in solution gradients and large elements in the other regions where the change in the solution gradients is small. The combined technique is used to improve the efficiency of the finite-element flow solution and the accuracy of the aerothermal loads, as well as to reduce the computational time and the computer memory. The Galerkin finite-element method is applied to solve the structural energy equation for temperature distribution and the structural equations for deformation and stress. The paper starts by explaining the theoretical formulation of high-speed compressible flow, structural heat transfer, and structural response. Then the solution procedure for flow-thermal-structural interaction problem is presented. The basic idea behind the adaptive meshing technique is then described. The efficiency of the combined procedure, the cell-centered finite-element method and the adaptive meshing technique, is evaluated by solving the Mach 4 flow past a flat plate and comparing results with those obtained from the finite-difference method. The high-speed flow, structural heat transfer, and deformation behaviors are then studied by applying the present method to Mach 10 flow past a flat plate to demonstrate their interdisciplinary coupling.

2. Theoretical Formulation and Solution Procedure

2.1 Governing equations:

The equations for the high-speed compressible

flow, the structural heat transfer, and the structural analysis in two dimensions are described below.

High-speed compressible viscous flow

The equations for high-speed compressible viscous laminar flow are represented by the conservation of mass, momentum, and energy. These equations are written in the conservation form (Hirsch, 1988) as

$$\frac{\partial}{\partial t}\{U_F\}+\frac{\partial}{\partial x}\{E_F\}+\frac{\partial}{\partial y}\{F_F\}=0 \tag{1}$$

where the subscript F denotes the fluid analysis. The vector $\{U_F\}$ contains the fluid conservation variables defined by

$$\{U_F\}=\begin{Bmatrix}\rho\\ \rho u\\ \rho v\\ \rho\varepsilon\end{Bmatrix} \tag{2}$$

where ρ is the fluid density, u and v are the velocity components in the x and y directions, respectively, and ε is the total energy. The vectors $\{E\}$ and $\{F\}$ consist of the flux components in the x and y directions, respectively (Dechaumphai and Limtrakarn, 1999).

Structural heat transfer

The thermal response of the structure is described by the energy equation in the conservation form as

$$\frac{\partial}{\partial t}U_T+\frac{\partial}{\partial x}E_T+\frac{\partial}{\partial y}F_T=G_T \tag{3}$$

where the subscript T denotes the structural heat transfer analysis. The vector U_T contains the thermal conservation variable defined by

$$U_T=\rho cT \tag{4}$$

where c is the specific heat of structure. The heat flux components E_T and F_T are

$$E_T=-k\frac{\partial T}{\partial x} \quad \text{and} \quad F_T=-k\frac{\partial T}{\partial y} \tag{5}$$

and G_T is the heat source.

Structural response

The structural response is governed by the quasi-static equilibrium equations given by

$$\frac{\partial}{\partial x}\{E_S\}+\frac{\partial}{\partial y}\{F_S\}=0 \tag{6}$$

where the subscript S denotes the structural analysis. The flux vector components $\{E_S\}$ and $\{F_S\}$ are

$$\{E_S\}=\begin{Bmatrix}\sigma_x\\ \tau_{xy}\end{Bmatrix} \quad \text{and} \quad \{F_S\}=\begin{Bmatrix}\tau_{xy}\\ \sigma_y\end{Bmatrix} \tag{7}$$

where the stress components σ_x, σ_y, and τ_{xy} are related to the strain and the temperature by the generalized Hook's law (Beer et al., 2002).

2.2 Finite-element formulation:

The cell-centered finite-element method is applied to the Navier-Stokes equations to derive the finite-element equations. The Galerkin finite element approach is applied to the structural heat transfer equation and the equilibrium equations to derive the corresponding finite-element equations. The derivation procedures are briefly described below.

Finite-element flow equations

The method of weighted residuals (Zienkiewicz and Taylor, 2000) is applied to Eq. (1) over the element domain, Ω, by using a unit interpolation function as

$$\int_\Omega\frac{\partial}{\partial t}\{U_F\}d\Omega=-\int_\Omega\frac{\partial}{\partial x}\{E_F\}d\Omega-\int_\Omega\frac{\partial}{\partial y}\{F_F\}d\Omega \tag{8}$$

The Gauss divergence theorem is then applied to the flux integral terms of Eq. (8) to yield,

$$\int_\Omega\frac{\partial}{\partial x}\{E_F\}d\Omega+\int_\Omega\frac{\partial}{\partial y}\{F_F\}d\Omega=\int_{\Gamma e}\Big(\{G_I\}+\{G_V\}\Big)\cdot\hat{n}\,d\Gamma \tag{9}$$

where the flux vectors $\{G_I\}$ and $\{G_V\}$ are the inviscid and viscous flux vectors of $\{E_I+F_I\}$ and $\{E_V+F_V\}$, respectively, and $\hat{n}$ is the unit vector normal to the element boundary, Γ_e. Equation (9) is evaluated by summing the normal fluxes from all sides, Γ_e, of the element. The fluxes normal to the element sides are then approximated by the numerical inviscid and viscous fluxes, $\{\bar{G}_I\}$ and $\{\bar{G}_V\}$. By applying an explicit time marching algorithm (Hirsch, 1988), Eq. (9) becomes

$$\frac{A_e}{\Delta t}\{U_F^{n+1}-U_F^n\}=-\sum_s\delta_s(\{\bar{G}_I\}+\{\bar{G}_V\}) \tag{10}$$

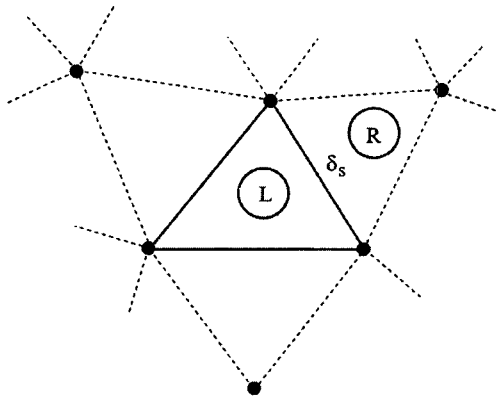

Fig. 1 The side length, δ_S, between the left element Ⓛ and right element Ⓡ.

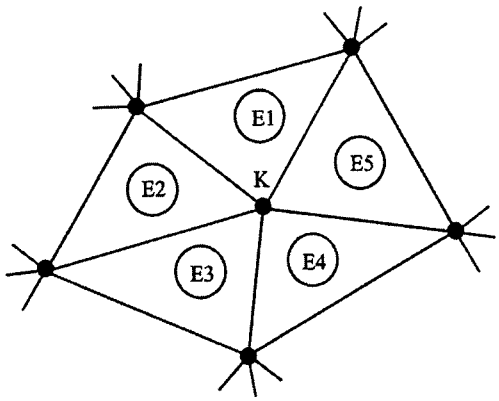

Fig. 2 Node K is surrounded by a number of elements

where U_F^{n+1} and U_F^n are the conservation variables at the time steps $n+1$ and n, respectively; A_e is the element area; δ_S is the length of the element side being considered as shown in Fig. 1 and the summation is performed for all sides. Δt is the allowable time step following the CFL and viscous stability requirement (Dechaumphai and Limtrakarn, 1999).

The basic concept behind the cell-centered finite-element method used in this paper is to determine the flux across element interfaces by using the Roe's averaging procedure. The average inviscid flux, $\bar{G}_I$, is given by

$$\bar{G}_I=\frac{1}{2}[G_I^L+G_I^R+|A^*|(U_F^L-U_F^R)] \qquad (11)$$

where the superscripts L and R denote the left and right elements, respectively. The last term in Eq. (11) may be viewed as an artificial diffusion needed for the solution stability. This diffusion is represented by the product of the Jacobian matrix $[A^*]$ and the difference between the left and right element conservation variables U_F^L and U_F^R (Limtrakarn and Dechaumaphai, 2003).

The average viscous flux, $\bar{G}_V$, in Eq. (10) normal to the element edge and its components consist of the stress and heat flux components that are in the form of the first-order derivative of u, v, and T (Hirsch, 1988). These derivative terms are computed from the nodal variable gradients. As an example, the temperature gradient at node K in Fig. 2, $\partial T_K/\partial x$, can be determined as follows. First, the temperature gradient of an element can be expressed as,

$$\frac{\partial T}{\partial x}=\lfloor N\rfloor\left\{\frac{\partial T}{\partial x}\right\} \qquad (12)$$

where $\lfloor N\rfloor$is the element interpolation function matrix. The method of weighted residuals is applied to Eq. (12) to yield,

$$\int_\Omega\{N\}\frac{\partial T}{\partial x}d\Omega=\int_\Omega\{N\}\lfloor N\rfloor\left\{\frac{\partial T}{\partial x}\right\}d\Omega \qquad (13)$$

Integration by parts is then applied to the integral term on the left-hand-side of Eq. (13).

$$[M]\left\{\frac{\partial T}{\partial x}\right\}=\int_{\Gamma_e}\hat{n}\,T_S\{N\}d\Gamma-\int_\Omega\left\{\frac{\partial N}{\partial x}\right\}T\,d\Omega \qquad (14)$$

where T_S is the temperature of the boundary, and

$$[M]=\int_\Omega\{N\}\lfloor N\rfloor d\Omega \qquad (15a)$$

For the explicit algorithm, the consistent matrix, $[M]$, in Eq. (15a) is written in the form of the lumped mass matrix, $[M]_{\text{lumped}}$, given by,

$$[M]_{\text{lumped}}=\frac{A_e}{3}\begin{bmatrix}1&0&0\\0&1&0\\0&0&1\end{bmatrix} \qquad (15b)$$

Then, Eq. (14) becomes,

$$(M_{\text{lumped}})_K\left.\frac{\partial T}{\partial x}\right|_K=\int_{\Gamma_e}\hat{n}\,T_S N_K\,d\Gamma-\int_\Omega\frac{\partial N_K}{\partial x}T\,d\Omega \qquad (16)$$

Also, the average temperature gradient at node K is computed from the contribution of the surrounding elements as,

$$\sum_E (M_{\text{lumped}})_K \left.\frac{\partial T}{\partial x}\right|_K = \sum_E \int_{\Gamma_e} \hat{n}_S N_K \, d\Gamma - \sum_E \int_\Omega \frac{\partial N_K}{\partial x} T \, d\Omega \quad (17)$$

The other derivative terms needed for computing the stress and heat flux components can be derived using the same procedure above.

By substituting Eq. (11) into Eq. (10), then Eq. (10) becomes

$$\frac{A_e}{\Delta t}\{U_F^{n+1} - U_F^n\} = -\frac{1}{2}\sum_S \delta_S [\{G_I^L\} + \{G_I^R\} + |A^*|(\{U_F^L\} - \{U_F^R\})] - \sum_S \delta_S \{\bar{G}_V\} \quad (18)$$

Finite-element structural heat transfer equations

The method of weighted residuals is applied to Eq. (3), over the element domain, Ω, by assuming a linear distribution of the conservation variable, U_T, and the flux components E_T and F_T in the form,

$$U_T(x, y, t) = \lfloor N(x, y) \rfloor \{U_T(t)\} \quad (19a)$$

$$E_T(x, y, t) = \lfloor N(x, y) \rfloor \{E_T(t)\} \quad (19b)$$

$$F_T(x, y, t) = \lfloor N(x, y) \rfloor \{F_T(t)\} \quad (19c)$$

where $\lfloor N(x, y) \rfloor$ is the linear interpolation function matrix. The finite-element equations can then be derived in the form:

$$[M]\{\Delta U_T\}^{n+1} = \{R_T\}_1^n + \{R_T\}_2^n \quad (20)$$

where $[M]$ is the mass matrix, and $\{\Delta U_T\}^{n+1} = \{U_T\}^{n+1} - \{U_T\}^n$ at time $n+1$. The $\{R_T\}_1^n$ and $\{R_T\}_2^n$ vectors are associated with the therma l fluxes within each element and across the element boundary, respectively, and are given by,

$$\{R_T\}_1^n = \int_\Omega \left\{\frac{\partial N}{\partial x}\right\} \lfloor N \rfloor d\Omega \{E_T^n\} + \int_\Omega \left\{\frac{\partial N}{\partial y}\right\} \lfloor N \rfloor d\Omega \{F_T^n\} \quad (21)$$

$$\{R_T\}_2^n = -\int_{\Gamma_e} \{N\}(E_T^n n_x + F_T^n n_y) \, d\Gamma \quad (22)$$

Finite-element structural equations

The Galerkin finite-element method is applied to Eq. (6) in the same fashion as in the structural heat transfer analysis. The finite-element equations can also be derived in the form:

$$[K]\{U_S\} = \{R_S\} + \{R_T\} \quad (23)$$

where $[K]$ is the stiffness matrix, $\{U_S\}$ is the nodal displacement vector, $\{R_S\}$ is the external load vector, and $\{R_T\}$ is the thermal load vector. These matrices are defined by

$$[K] = \int_\Omega [B]^T [C][B] \, d\Omega \quad (24)$$

$$\{R_S\} = \int_{\Gamma_e} [N]^T \{F_S\} \, d\Gamma \quad (25)$$

$$\{R_T\} = \int_\Omega [B]^T [C]\{\alpha\}(T - T_0) \, d\Omega \quad (26)$$

where $[B]$ is the strain-displacement interpolation matrix, $[C]$ is the elastic modulus matrix, $\{F_S\}$ is the surface traction matrix, $\{\alpha\}$ is the thermal expansion coefficient vector, and T_0 is the reference temperature for zero stress state.

2.3 Solution sequence

For high-speed compressible flows, the flow behavior normally approaches a steady state much faster than that of the thermal and structural response of the structure. Typically, the heating rate approaches a steady state in about few milliseconds. At this time, the structural configuration remains nearly undeformed at a temperature only slightly higher than the initial temperature. After few seconds, the structural temperature begins to rise appreciably and significant deformation may occur. At this time, thermal and deformation coupling effect can alter the flow field. The coupling effect continues to alter the flow and structure behavior until the structure reaches the state of the thermal equilibrium.

Based on the fact that the high-speed flow behavior normally reaches the steady-state condition in a much shorter time than the structural response, the analysis procedure of the flow-structure interaction presented in this paper consists of the solution sequence as described by Fig. 3. This solution sequence can reduce the total computational time by avoiding detailed transient flow analysis that requires significant computational effort (Limtrakarn, 2003). At the initial time, $t = t_0$, the adaptive cell-centered finite-element method is first used to predict the high-speed flow behavior as denoted by FA (Flow Analysis). The flow analysis generates aerothermal loads that include heating rate and pressure along the structural surface. After a short interval of time at $t = t_1$, the predicted aerodynamic heat-

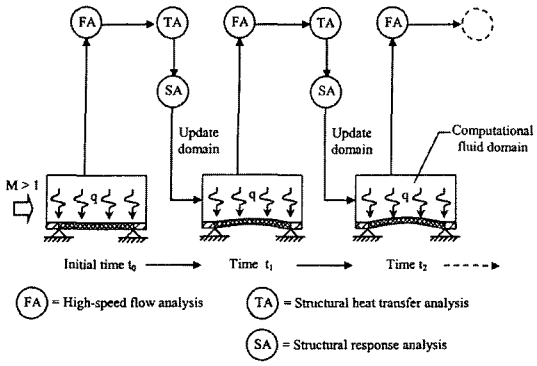

Fig. 3 Solution sequence of flow-structure interaction for high-speed flow over a flat plate

ing rate is applied to the structural configuration and the structural heat transfer analysis as denoted by TA (Thermal Analysis) is used to solve the structural temperature. Both the structural temperature and the fluid pressure are then used to predict the structural response for deformation and stresses as denoted by SA (Structural Analysis). The same sequence is repeated to predict the new flow field behavior, the aerothermal loads, the structural temperature, as well as the new structural deformation and stresses.

3. Adaptive Meshing Technique

Adaptive mesh generation techniques may be classified into two major categories: 1) refinement/derefinement, and 2) remeshing. The first category, the adaptive refinement/ derefinement technique, can be further classified into three subcategories: a) the h method, b) the p method, and c) the r method. In the h method, the elements in the initial mesh are refined into smaller elements or derefined into larger elements (Ramakrishnan et al., 1990). The p method maintains the geometry of the elements of the initial mesh but increases (or decreases) the order of the polynomials used for the element interpolation functions (Dechaumphai, 1982). The r method keeps the number of elements and their connectivities the same but relocates the nodes (Lohner et al., 1984).

The remeshing technique, the second adaptive mesh-generation category, generates an entirely new mesh based on the solution obtained from an earlier mesh (Dechaumphai, 1995; Peraire et al., 1987). The technique is combined with the cell-centered finite-element method in this paper to obtain solutions of high-speed compressible flow problems. The idea is to construct a new mesh that consists of small elements in the regions with large change in solution gradients and large elements in the other regions where the changes in the solution gradients are small. As an example, small elements are needed in the regions of shock waves to capture shock resolution, whereas larger elements can be used in the free-stream region because the flow behavior is uniform. To determine proper element sizes at different locations in the flow field, the solid-mechanics concept of determining the principal stresses from a given state of stresses at a point is employed. Since the fluid density changes abruptly across the shock waves, thus the density distribution can be used as an indicator for the determination of proper element sizes.

Because small elements must be placed in the region of the shock wave where large changes in the density gradient occur, the second derivatives of the density at a point with respect to global x and y coordinates are needed to compute,

$$\begin{bmatrix} \dfrac{\partial^2\rho}{\partial x^2} & \dfrac{\partial^2\rho}{\partial x\partial y} \\ \dfrac{\partial^2\rho}{\partial x\partial y} & \dfrac{\partial^2\rho}{\partial y^2} \end{bmatrix} \tag{27}$$

Then the principal quantities in the principal X and Y directions, where the cross-derivatives vanish, are determined,

$$\lambda_1=\left|\frac{\partial^2\rho}{\partial X^2}\right| \quad \text{and} \quad \lambda_2=\left|\frac{\partial^2\rho}{\partial Y^2}\right| \tag{28}$$

These principal quantities are then used to compute proper element sizes, h_1 and h_2, in the two principal directions using the following condition (Oden and Carey, 1981),

$$h_1^2\lambda_1=h_2^2\lambda_2=\text{constant}=h_{\min}^2\lambda_{\max} \tag{29}$$

where $h_{\min}$ is the specified minimum element size, and $\lambda_{\max}$ is the maximum principal quantity for the entire model.

Based on the condition in Eq. (29), the element

sizes are generated according to the given minimum element size h_{min}. Specifying too small h_{min} may result in a model with an excessive number of elements. On the other hand, specifying too large h_{min} may result in an inadequate solution accuracy or excessive analysis and meshing cycles. These factors must be considered prior to generating a new mesh. Note that, because the technique generates an entirely new mesh with different nodal locations from the old mesh, interpolation of the solution from the old to the new mesh should be used to increase the analysis solution convergence.

4. Applications

A Mach number 4 flow past a flat plate is presented as the first example to validate the adaptive cell-centered finite-element method for high-speed flow analysis and to compare the results with those obtained from the finite-difference method. Then the performance of the proposed high-speed flow-structure interaction procedure is evaluated by Mach number 10 flow past a flat plate.

4.1 Mach 4 flow past a flat plate :

The problem statement of a mach 4 flow past a flat plate as shown in Fig. 4 was taken from a reference (Anderson, 1995) that presents the analysis solution by using the finite-difference method. The flow enters through the left boundary of the computational fluid domain. The shock wave is created from the leading edge as highlighted in the figure. The inlet flow conditions consist of specifying ρ=1.2252kg/m^3, u=1,361m/s, v=0, ε=1,133,080J/kg, Re=932 with the wall temperature of 288.16K. The combined method of the cell-centered finite-element analysis and the adaptive meshing technique is applied to solve the problem. Figure 5(a) shows the final adaptive mesh that consists of small elements clustered along the shock line from the sharp leading edge. The accuracy of the shock resolution and the shock angle strongly depends on the finite element mesh near the sharp leading edge. To capture the aerodynamic heating rate accurately, graded quadrilateral elements normal to the flat plate are generated to capture the thin boundary layer along the flat plate and in the leading edge region as shown in the figure. The total of 10,353 triangular elements are generated in the inviscid region and 4,011 quadrilateral elements in the boundary layer. Figure 5(b) shows the predicted density contours with high value at the leading edge.

As the flow encounters the leading edge, the fluid particles stop at the leading edge stagnation point. The oncoming freestream thus sees the leading edge as a blunt body. A viscous boundary layer region is then created between the plate and the induced shock wave. The lost kinetic energy from viscous dissipation then transforms into the internal energy, causing aerodynamic heat transfer rate and changing flow field temperature in the boundary layer region.

The predicted u-velocity distribution is normalized with the freestream velocity, u_∞, and

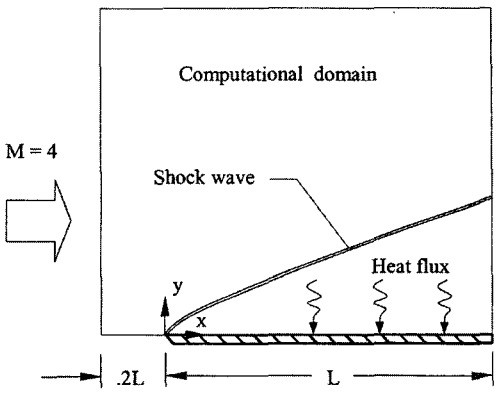

Fig. 4 Mach 4 flow past a flat plate

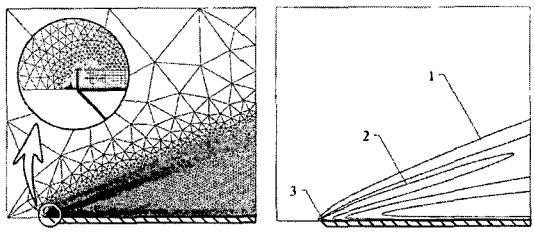

(a) Final adaptive mesh (b) Density distribution(kg/m^3)

Fig. 5 Final adaptive mesh and corresponding density contours for mach 4 viscous flow past a flat plate

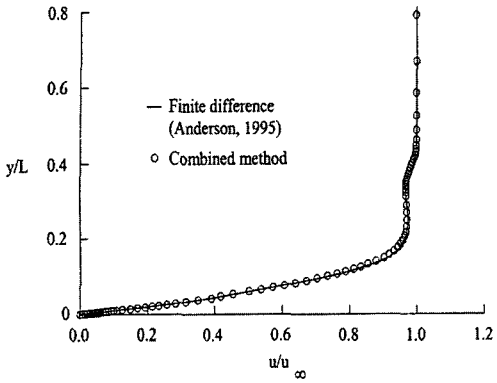

Fig. 6 Comparative normalized u-velocity distributions along normalized y distance at the flow exit $(x=L)$ for mach 4 viscous flow past a flat plate

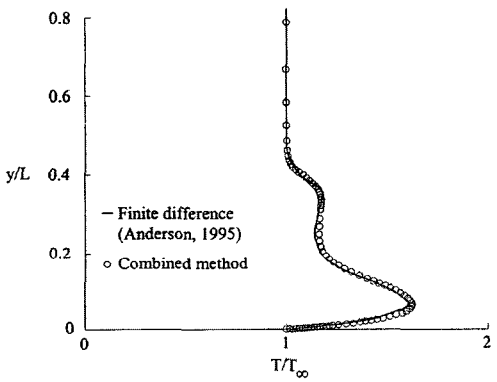

Fig. 7 Comparative normalized temperature distributions along normalized y distance at the flow exit $(x=L)$ for mach 4 viscous flow past a flat plate

compared with the finite difference solution along the y-direction at the flow exit as shown in Fig. 6. The figure shows good agreement between the finite-element and the finite-difference solutions. At the flow exit, the u-velocity decreases slightly across the plate shock wave, and then reduces abruptly within the thin boundary layer to zero at the plate surface.

The predicted temperature distribution is normalized and compared with the finite difference solution along the y-direction at the same flow exit location as shown in Fig. 7. The figure shows the flow temperature increases slightly across the plate shock wave. The flow temperature then increases again before decreasing rapidly to the plate temperature within the thin boundary layer. Such steep flow temperature gradient next to the plate thus introduces aerodynamic heating rate on the plate.

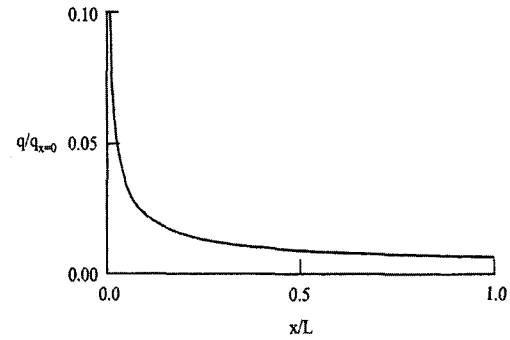

Fig. 8 Predicted heating rate distribution along the plate for mach 4 viscous flow past a flat plate

The comparison between the two solutions shows good agreement with high temperate gradient in the thin thermal layer near the plate. The predicted flow temperature for the elements near the plate is also used to compute the temperature gradient and then the heating rate that occurs on the plate. Figure 8 shows the computed heating rate distribution along the plate, showing high value at the leading edge. Small quadrilateral elements are needed in the thin boundary layer to provide accurate heating rate solution. The example highlights the benefit of the adaptive meshing technique that can generate proper element sizes automatically to provide high solution accuracy with reduced total number of unknowns and thus the computational time.

4.2 Mach 10 flow past a flat plate :

The performance of the high-speed flow-structure interaction analysis procedure is evaluated by the example of Mach 10 flow past a flat plate as illustrated in Fig. 9. The flow enters through the left boundary of the computational fluid domain and creates a shock wave from the leading edge as highlighted in the figure. The inlet flow conditions consist of specifying ρ=4.303E-05kg/m^3, u=1,418.7m/s, v=0, ε=1,043,000J/kg, Re=5,580 with the wall temperature of 288.16K. The flow-thermal-structural interaction of the flat plate was analyzed using the solution sequence

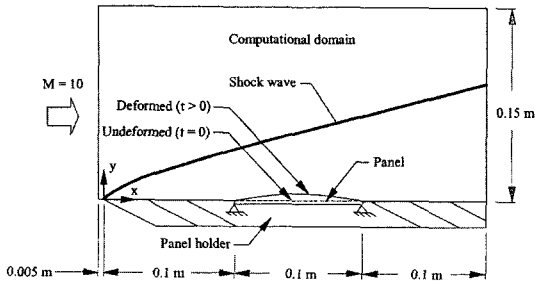

(a) Problem statement

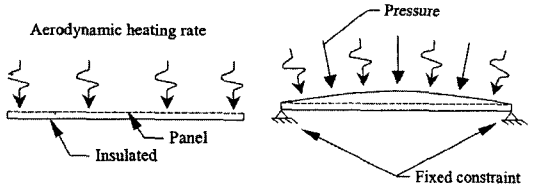

(b) Boundary condition for heat transfer analysis (c) Boundary condition for structural analysis

Fig. 9 Mach 10 flow past a flat plate

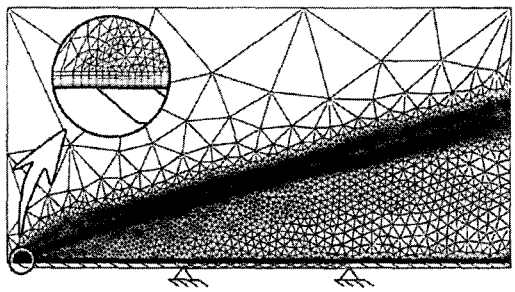

(a) Adaptive mesh

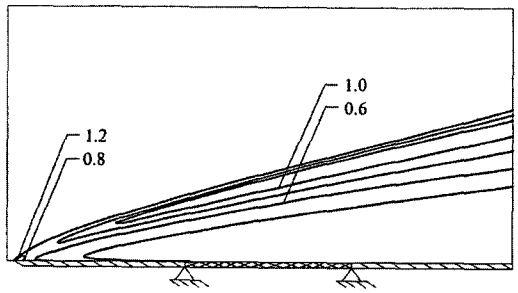

(b) Density distribution ($x10^{-4}$kg/m^3)

Fig. 10 Adaptive mesh and corresponding density contours for Mach 10 flow past a flat plate at $t=0$ sec

shown in Fig. 3. At the initial time, $t=0$ second, the flow field behavior is predicted by using the cell-centered finite-element method. Based on this flow solution, the adaptive meshing technique as described in the preceding section is then applied to obtain the adaptive mesh as shown in Fig. 10(a). Small elements are automatically generated along the shock line to improve shock resolution and larger elements in other regions. A total of 13,727 triangular elements are generated in the inviscid region and 7,560 quadrilateral elements inside the boundary layer. Ten graded layers of quadrilateral elements are used inside the boundary layer to capture steep temperature gradients for the accurate aerodynamic heating rate prediction. The predicted flow solution is shown by the density contours in Fig. 10(b). With the predicted aerodynamic heating rate from the flow analysis at time $t=2$ seconds, the structural heat transfer analysis is used to predict the temperature distribution on plate surface between $0.1<x<0.2$m. At the same time, the quasi-static structural analysis is performed to compute the corresponding structural deformation. The computational fluid domain is then updated by the deformed plate and the cell-centered finite-element method is applied to predict the new flow field behavior. The adaptive meshing technique is again applied to generate the new adaptive mesh as shown in Fig. 11(a). The shock pattern is altered by the convex deformation of the plate surface while small elements are automatically clustered to capture the new shock pattern. The corresponding fluid density contours are shown in Fig. 11(b). The fluid density increases through the shock wave and decreases as the fluid flows across the convex center of the plate along the left support toward the right support. The entire analysis procedure is repeated to compute the plate deformation shape and the new flow field behavior at time $t=4$ seconds as shown in Fig. 12. The figure shows the development of the shock emanating from the left support on the windward side of the deformed plate. As the plate deforms into the flow field, the boundary layer thickness is altered over the plate, becoming thinner after the flow encounters the left support and then it is thicker as the flow approaches the right support of the plate. Figures 13 and 14 compare the predicted aerodynamic heating rates and the pressures, respectively, for $0<x<\langle 0.3$m. The effect of both the fluid/plate heat transfer and

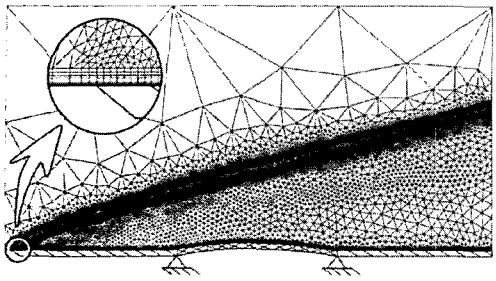

(a) Adaptive mesh

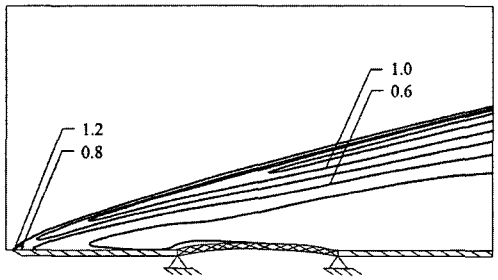

(b) Density distribution ($x10^{-4}$kg/m^3)

Fig. 11 Adaptive mesh and corresponding density contours for Mach 10 flow past a flat plate at $t=2$ sec

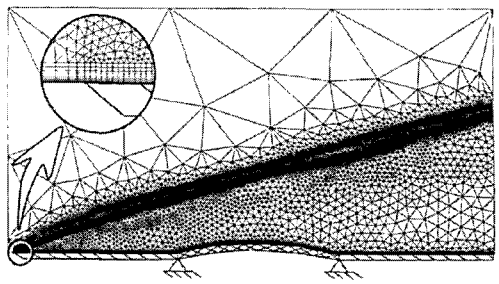

(a) Adaptive mesh

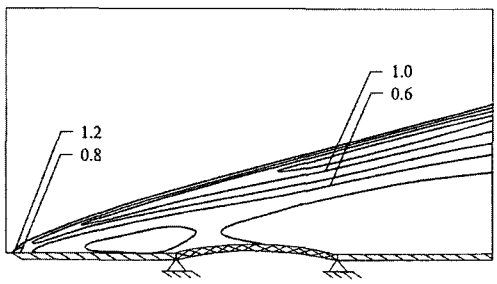

(b) Density distribution ($x10^{-4}$kg/m^3)

Fig. 12 Adaptive mesh and corresponding density contours for Mach 10 flow past a flat plate at $t=4$ sec

the plate deformation causes the heating rate and the pressure to increase for $0.1<x<0.2$ as shown in the figures. The change in heating rates at $x=$ 0.1 and 0.2m. is associated with the boundary thinning and thickening, respectively. These figures highlight the interdisciplinary coupling between the flow field and the deformed plate. The heated plate can deform into the flow field, and at the same time, the altered flow field can change the aerothermal loads of the heating rate and the pressure on the plate.

5. Concluding Remarks

The multidisciplinary interaction behaviors of high-speed compressible flow, structural heat transfer, and structural response were presented using the adaptive finite-element method. The finite-element method based on the cell-centered algorithm was used to predict the high-speed compressible flow behavior. The method was combined with the adaptive meshing technique to improve the flow accuracy. The technique generates an entirely new mesh based on the solution obtained from the previous mesh. The new mesh consists of the clustered elements in the region with large change in the solution gradients to provide the high accuracy, and large elements are generated in the other regions to minimize the computational time and computer memory. The Galerkin finite-element method was used to predict the structural heat transfer and structural response behaviors. The finite-element formulation, the computational procedure and the basic idea behind the adaptive meshing technique were described. The Mach 4 flow past a flat plate was the first example used to validate the high-speed flow solution by comparing results with those obtained from the finite-difference method. Both solutions were found to be in good agreement. The Mach 10 flow past a flat plate was then used to study the flow-structure interaction and to evaluate the performance of the proposed analysis procedure. The later example highlights the interaction behavior between the high-speed flow and the thermal-structural response of the structure. These examples demonstrate the capability of the proposed high-speed compressible viscous

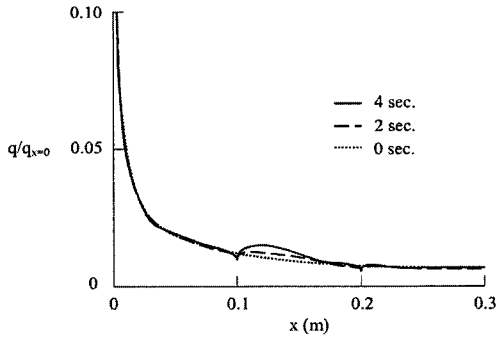

Fig. 13 Heat flux distributions for Mach 10 flow past a flat plate

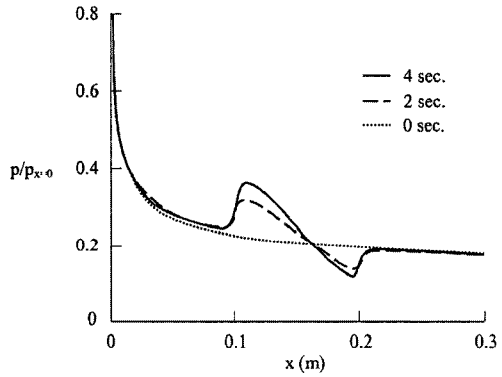

Fig. 14 Pressure distributions for Mach 10 flow past a flat plate

flow and the thermal-structural analysis methods for simulating fluid-structure interaction behavior.

Acknowledgement

The authors are pleased to acknowledge Thailand Research Fund (TRF) for supporting this research work.

References

Anderson, J. D. Jr., 1982, Modern Compressible Flow With Historical Prospective, New York : McGraw-Hill.

Anderson, J. D. Jr., 1991, Fundamentals of Aerodynamics, Second Ed., New York : McGraw-Hill.

Anderson, J. D. Jr., 1995, Computational Fluid Dynamics, McGraw-Hill, New York.

Aftosmis, M. J. Berger, M. J. Adomavicius, G., 2000, "A Parallel Multilevel Method for Adaptively Refined Cartesian Grids with Embedded Boundaries," AIAA Paper 2000-0808.

Baek, S-C. Kwon, S-B. Lee, B-E, 2003, "An Experimental Study of Supersonic Dual Coaxial Free Jet," *KSME International Journal* Vol. 17 No. 12 : pp. 2107~2115.

Baum, J. D., 2002, "Development of a Coupled CFD/CSD Methodology using an Embedded CSD Approach," Conference on Computational Physics.

Beer, F. P., Johnston, E. R., DeWolf, J. T., 2002, Mechanics of Materials, Third Edition, New York : McGraw-Hill.

Dechaumphai, P., 1982, "Improved Finite Element Methodology for Integrated Thermal-Structure Analysis," NASA CR 3635.

Dechaumphai, P., 1995, "Adaptive Finite Element Technique for Heat Transfer Problems," *Journal of Energy, Heat & Mass Transfer*, Vol. 17, No. 2, pp. 87~94.

Dechaumphai, P. Limtrakarn, W., 1999, "Adaptive Cell-Centered Finite Element Technique for Compressible Flows," *Journal of Energy, Heat and Mass Transfer*, Vol. 21, pp. 57~65.

Glass, D. E., Merski, N. R., Glass, C. E., 2002, "Airframe Research and Technology for Hypersonic Airbreathing Vehicles," AIAA Paper 2002-5137.

Gnoffo, P. A., 1986, "Application of Program LAURA to Three-dimensional AOTV Flowfields," AIAA Paper 86-0565.

Hirsch, C., 1988, Numerical Computation of Internal and External Flows. Vol. 1, New York : Wiley.

Kang, H.-K. Tsutahara, M. Ro, K.-D. Lee, Y.-H., 2003, "Numerical Analysis of a Weak Shock Wave Propagating in a Medium Using Lattice Boltzmann Method (LBM)," *KSME International Journal* Vol. 17 No. 12 : pp. 2034~2041.

Kim, H-D. Kashimura, H. Setoguchi, T., "The Self-Induced Oscillations of the Under Expanded Jets Impinging Upon a Cylindrical Body," *KSME Iternational Journal* Vol. 16 No. 11 : pp. 1448~1456.

Limtrakarn, W., 2003, Finite Element Method

for High-Speed Flow-Structure Interaction, PhD thesis, Mechanical Engineering Department, Chulalongkorn University.

Limtrakarn, W. Dechaumphai, P., 2003, "Computations of High-Speed Compressible Flows with Adaptive Cell-Centered Finite Element Method," *J Chin Inst Eng*, Vol. 26 : pp. 553~563.

Lohner, R., Morgan, K., Zienkiewicz, O. C., 1984, "Adaptive Grid Refinement for Compressible Euler and Navier-Stokes Equations," The International Conference on Accuracy Estimates and Adaptive Refinements in Finite Element Computations, Vol. 2 : pp. 189~202, New York : Wiley.

Lohner, R. Baum, J. D. Mestreau, E. Sharov, D. Charman, C. Pelessone, D., 2003, "Adaptive Embedded Unstructured Grid Methods," AIAA Paper 03-1116.

Oden, J. T. Carey, G. F., 1981, Finite Elements : Mathematical Aspects. New Jersey : Prentice-Hall.

Peraire, J. Vahjdati, M., Morgan, K., Zienkiewicz, O. C., 1987, "Adaptive Remeshing for Compressible Flow Computation," *J Comput Phys*, Vol. 72, pp. 449~466.

Ramakrishnan, R., Bey, K. S., Thornton, E., 1990, "A Adaptive Quadrilateral and Triangular Finite-Element Scheme for Compressible Flows," *AIAA Journal*, Vol. 28, No. 1, pp. 51~59.

Zienkiewicz, O. C. Taylor, R. L., 2000, The Finite Element Method. Fifth Ed., Woburn : Butterworth-Heinemann.